Dynamic manipulation and separation of individual semiconducting and metallic nanowires

ARASH JAMSHIDI[1†], PETER J. PAUZAUSKIE[2,3†‡], P. JAMES SCHUCK[4], AARON T. OHTA[1], PEI-YU CHIOU[5], JEFFREY CHOU[1], PEIDONG YANG[2,3]* AND MING C. WU[1]*

[1]Department of Electrical Engineering, University of California, Berkeley, California 94720, USA
[2]Department of Chemistry, University of California, Berkeley, California 94720, USA
[3]Materials Science Division, Lawrence Berkeley National Laboratory, Berkeley, California 94720, USA
[4]Molecular Foundry, Lawrence Berkeley National Laboratory, Berkeley, California 94720, USA
[5]Department of Mechanical and Aerospace Engineering, University of California, Los Angeles (UCLA), Los Angeles, California 90095, USA
[†]These authors contributed equally to this work.
[‡]Present address: Chemistry, Materials, and Life Sciences Directorate, Lawrence Livermore National Laboratory, 7000 East Avenue, L-235, Livermore, California 94551
*e-mail: p_yang@berkeley.edu; wu@eecs.berkeley.edu

The synthesis of nanowires has advanced in the past decade to the point where a vast range of insulating, semiconducting and metallic materials[1] are available for use in integrated, heterogeneous optoelectronic devices at nanometre scales[2]. However, a persistent challenge has been the development of a general strategy for the manipulation of individual nanowires with arbitrary composition. Here we report that individual semiconducting and metallic nanowires with diameters below 20 nm are addressable with forces generated by optoelectronic tweezers[3]. Using 100,000 times less optical power density than optical tweezers, optoelectronic tweezers are capable of transporting individual nanowires with speeds four times greater than the maximum speeds achieved by optical tweezers. A real-time array of silver nanowires is formed using photopatterned virtual electrodes, demonstrating the potential for massively parallel assemblies. Furthermore, optoelectronic tweezers enable the separation of semiconducting and metallic nanowires, suggesting a broad range of applications for the separation and heterogeneous integration of one-dimensional nanoscale materials.

One approach for the organization of materials with nanometre-scale dimensions[4] is the so-called 'bottom-up' assembly of heterogeneous building blocks[5]. Although it is possible to achieve a high level of orientation control[6,7] through epitaxial growth of semiconductor materials[8], there are enormous challenges to achieving a high level of integration with heterogeneous material systems owing to large differences in chemical and thermal stability. One way to circumvent the constraints of thermochemical incompatibility is first to synthesize the various materials in favourable processing conditions, then to apply a strategy for post-synthesis integration.

Several techniques have been used over the past decade to enable nanowire integration. Advances in microcontact printing have opened up the possibility to coat macroscopically large areas with inorganic nanowires or carbon nanotubes[9]. Microfluidic[10,11] and Langmuir–Blodgett[12–14] patterning have also been used to align large numbers of nanowires dispersed in a fluid matrix. The manipulation of single structures requires more precise control, which has been achieved using motorized nanomanipulators[15] or optical traps[16]. Dielectrophoresis[17–19] (DEP) is another approach that has been used recently to manipulate suspended one-dimensional (1D) nanostructures. In this technique, microfabricated electrodes are used to produce an a.c. potential that polarizes the given 1D nanostructure, forcing it to align with the electric-field lines between the patterned electrodes. The non-uniform electric field present in the liquid layer induces a dipole in the nanostructures and attracts them to the region of highest field gradient. The DEP force expression for a spherical particle[20] is given by $F_{DEP} = 2\pi r^3 \varepsilon_m \mathrm{Re}(K)\nabla E^2$, where r is the radius of the particle, ε_m is the permittivity of the media, Re (K) is the real part of the Clausius–Mossotti factor (K), and ∇E^2 is the gradient of the squared electric field. The Clausius–Mossotti factor is a function of the permittivity and conductivity of the particle and the media and, in the case of spherical particles, has a value between -0.5 and 1. Although the approach has yielded impressive nanostructure alignment[18] and separations[17], it is constrained because the DEP electrodes are fixed in place and it is not possible to arrange individual nanostructures into real-time reconfigurable patterns.

Optoelectronic tweezers (OET) have emerged as a powerful tool for massively parallel manipulation of polymer beads and living cells at micrometre length scales through optically induced DEP (ref. 3). Two-dimensional (2D) patterns of low-intensity light are projected onto a plane of photoconductive material sandwiched between transparent parallel-plate electrodes. The light excites carriers in the photoconductive layer (hydrogenated amorphous silicon), reducing the local impedance to create an inhomogeneous electric field across the liquid layer. In the
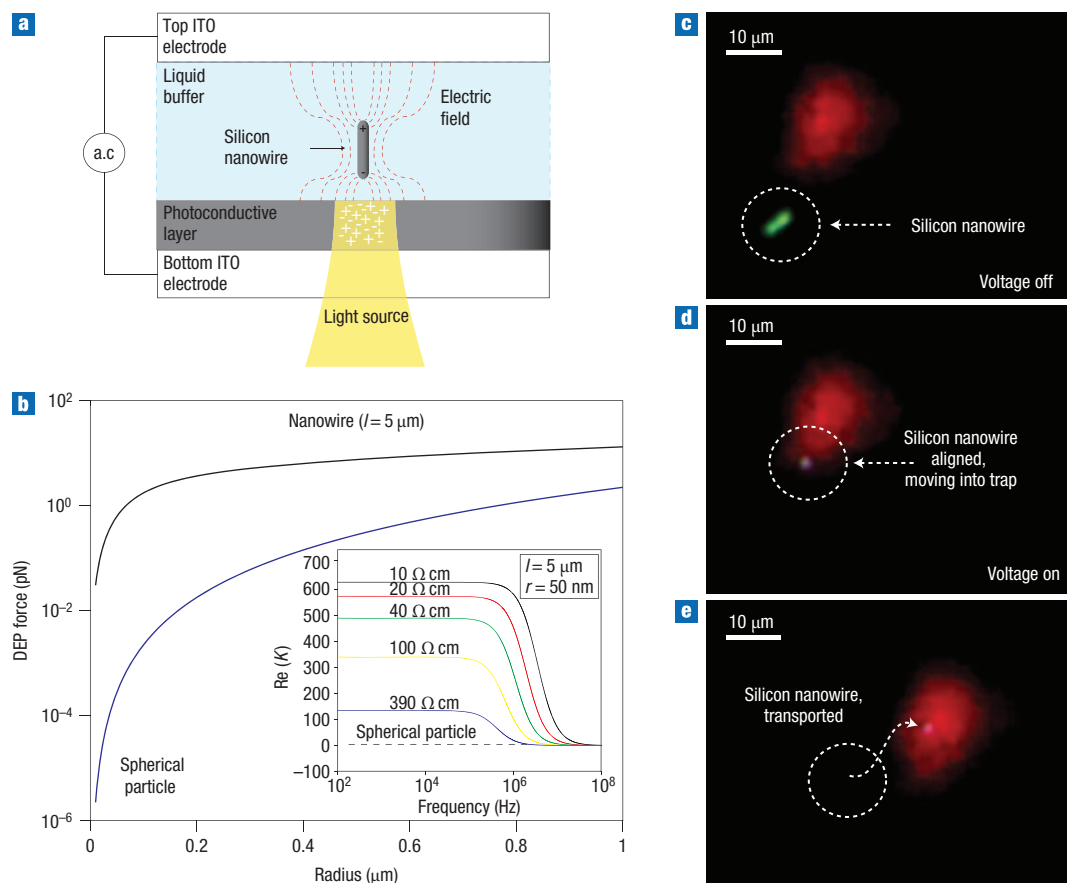
Figure 1 OET manipulation of single silicon nanowire. a, OET device structure with an individual nanowire trapped at the laser spot (ITO, indium tin oxide). **b**, Comparison of the DEP force for a 5-μm-long nanowire and a spherical particle as a function of radius. The inset shows the simulated values of Re (K) over a range of frequencies for different nanowire resistivities (for a nanowire of 5 μm length and 50 nm radius). **c–e**, Stages of trapping of an individual silicon nanowire using a laser spot: no voltage is applied across the device and the nanowire undergoes brownian motion (**c**); a voltage is applied, and the long axis of the nanowire aligns with the electric field and the nanowire moves into the trap (**d**); the nanowire follows the laser trap position (**e**).

presence of the non-uniform electric field, a polarization is induced in particles between the parallel plates. The polarized particles are either attracted to or repelled from the field gradient (as in DEP) produced by the projected light pattern, yielding a powerful optoelectronic method of particle manipulation based on dynamic, light-actuated virtual electrodes[21].

Although this approach works extremely well for micrometre-scale objects, the forces generated with OET typically are overcome by thermal (brownian) fluctuations when the particles are much smaller than 1 μm, as the DEP force scales with r^3. The theory of DEP trapping[20] suggests that one way to manipulate objects with submicrometre dimensions is to work with highly elongated structures, where two dimensions of the particle can be significantly below 100 nm, but the third dimension is of the order of micrometres. Modelling the force using an elongated ellipsoid model[20], the DEP force for a nanowire is given by $F_{DEP} = (\pi r^2 l/6)\varepsilon_m \text{Re}(K)\nabla E^2$, where r and l are the nanowire's radius and length, respectively. For nanowires that are much more polarizable than the surrounding media and have high aspect ratios K can be much larger than 1.

To determine whether OET forces could address nanowires suspended in a fluid matrix, we transferred an aqueous suspension of silicon nanowires to a device chamber as illustrated in F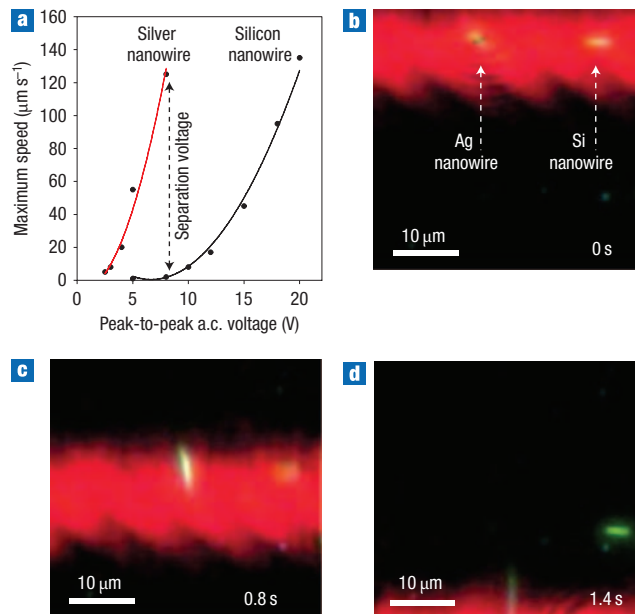ig. 1a. In addition, finite-element simulations were used to calculate approximate field gradients and the corresponding forces on suspended nanowires. In comparing the DEP force of a nanowire (length = 5 μm) and a spherical particle over a range of radii (Fig. 1b), it is evident that the nanowire experiences a DEP force 2–3 orders of magnitude larger than the spherical particle owing to one of the dimensions of the nanowire (length) being larger than the spherical particle and the increase in the value of K for the nanowire. The inset of Fig. 1b shows the simulated values of Re(K) for a nanowire of length 5 μm and radius 50 nm for different values of nanowire resistivity over a range of frequencies. As mentioned above, the smallest spherical particle trappable using OET has a diameter of approximately 1 μm. The increase in the DEP force for the nanowire, however, makes it possible to trap individual nanowires having diameters as small as 20 nm with OET. Nanowires experience a torque in addition to the DEP force, which aligns the long axis of the nanowire with the electric field perpendicular to the imaging plane of the OET device (Fig. 1a,d). Therefore, the nanowire is aligned vertically within the sample chamber. Figure 1c–e shows the process of trapping an individual silicon nanowire using a 633-nm HeNe laser (10 μm full-width at half-maximum (FWHM) and intensity 100 W cm^{-2}). In Fig. 1c there is no voltage applied across the device and the nanowire undergoes brownian motion (see Supplementary Information, Video S1).
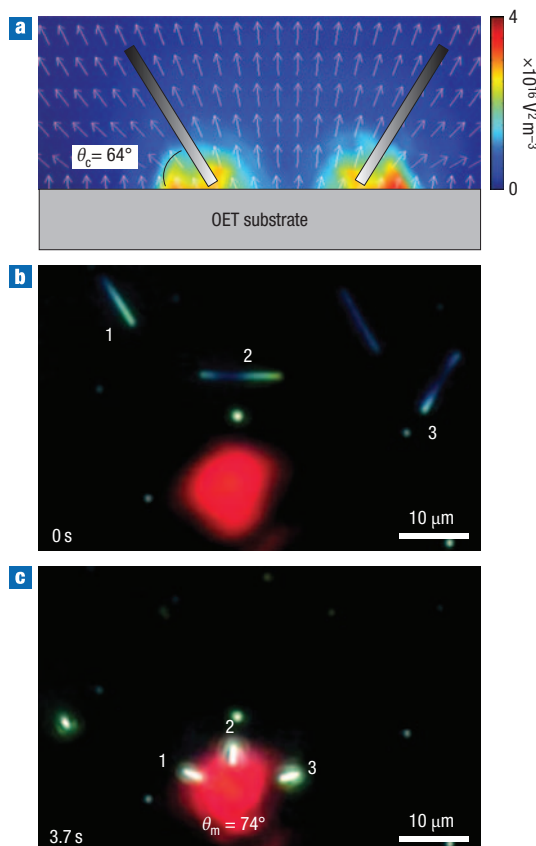
Figure 2 OET manipulation of silver nanowires. a, Simulation of ∇E^2 (colour plot) and the electric field (arrows) for a 50-kHz, 8-V peak-to-peak bias applied to the device. The electric field in the area of highest ∇E^2 (where the wires are trapped) is calculated to have an angle of $\theta_c = 64°$ with the OET surface. **b**, No voltage is applied to the device, and the silver nanowires undergo brownian motion and are not attracted to the laser spot. **c**, Once the voltage is turned on, the nanowires align with the electric field and are trapped in the laser spot at an angle of approximately $\theta_m = 74°$, which is within about 15% of the calculated value.


Figure 3 Dynamic separation of semiconducting and metallic nanowires. Process of separation of an individual silver nanowire from an individual silicon nanowire by adjusting the scanning speed of a line laser. **a**, Maximum experimental trapping speed for individual silicon and silver nanowires over a range of peak-to-peak a.c. voltages. Owing to the high polarizability of silver nanowires, at 8 V peak-to-peak, the silver nanowire experiences speeds up to 125 μm s^{-1} whereas the silicon nanowire only experiences speeds less than 2 μm s^{-1}. The solid lines in the plot are quadratic fits to the experimental data points. **b**, Both silver and silicon nanowires rest in the stationary trapping potential. **c**, The translation of the line potential begins the separation. **d**, Scanning of the laser line with speeds greater than 2 μm s^{-1} causes final separation of the silver and silicon nanowires.

Once the voltage is applied (Fig. 1d), the long axis of the nanowire aligns with the electric field in a fraction of a second and the nanowire follows the laser trap as the beam is manually scanned across the stage (Fig. 1e). Maximum trapping speeds for an individual silicon nanowire with 100-nm diameter and 5-μm length approach 135 μm s^{-1} with a peak-to-peak trapping voltage of 20 V. This is approximately four times the maximum speed achievable by optical tweezers[16] and is reached with 5–6 orders of magnitude less optical power density than optical tweezers.

In addition, the OET trap stiffness figure-of-merit[22] is measured to be 1.6×10^{-6} N m^{-1} mW^{-1}, which is approximately two orders of magnitude larger than typical trap stiffness figure-of-merit values reported for optical tweezers[16] (see Supplementary Information, Fig. S6). Fundamentally, the size of the trapping potentials is diffraction limited and the positioning accuracy of the wire inside the trap is limited by brownian motion. We used particle-tracking image analysis software to measure the nanowire localization to be less than 0.22 μm^2 (see Supplementary Information, Fig. S3). Although a single wire is trapped in this potential well, it is possible to trap

arbitrarily large numbers of wires in a given area, simply by focal adjustment of the optical spot's size (see Supplementary Information, Video S2).

We have also found it possible to preserve the position and orientation of the wires trapped with OET using a photocurable polymer[23,24] solution such as polyethylene glycol diacrylate[25,26] (PEGDA), enabling immobilization of nanowires in the polymer matrix within seconds by exposing the manipulation area to a UV source (see Supplementary Information, Fig. S7, Video S3). The ability to preserve the position and orientation of OET-trapped nanowires is critical for enabling later post-processing steps, such as the deposition of metallic contacts. The polymer solution's increased viscosity and conductivity are found to reduce the speed of nanowire translation by more than a factor of two, and future work will focus on finding optimal polymer solutions to minimize interference from viscous drag and the screening of nanowire polarizability.

In addition to trapping semiconductor nanowires, we also demonstrated that OET is capable of trapping and manipulating metallic (silver) nanowires. Earlier experiments with a single-beam infrared laser trap showed that high laser powers led to intense heating and scattering forces that prevented the optical trapping of silver nanowires[16]. Silver nanowires were found to show interesting OET trapping characteristics (Fig. 2) owing to their very high polarizability, which forces them to align strongly with the electric field present in the liquid layer. Figure 2b,c shows the process of trapping three silver nanowires over a
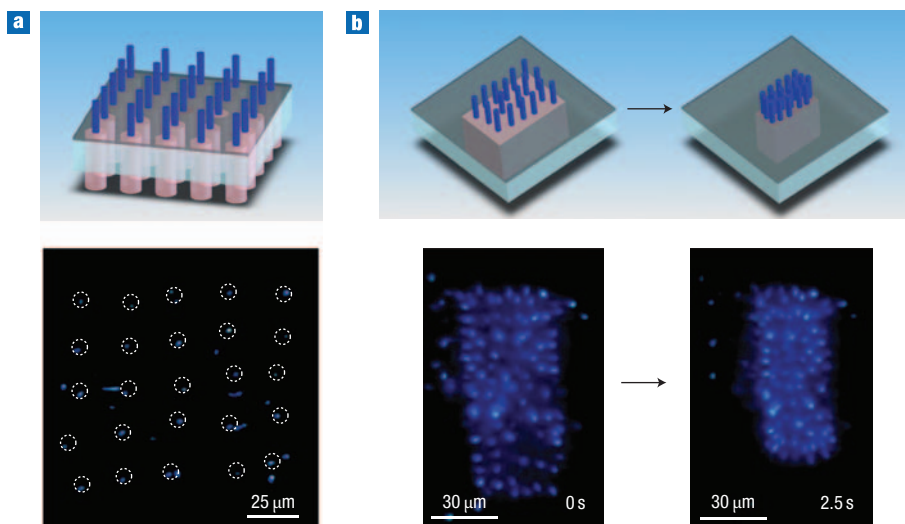
Figure 4 Large-scale assembly of nanowires. Large-scale manipulation of silver nanowires using traps created with a digital micromirror spatial light modulator and positioned with a computer-mouse-controlled graphical user interface. **a**, Formation of a 5×5 single silver nanowire array. **b**, Large-scale control of nanowire density by adjusting the size of the trapping pattern. A collection of more than 80 silver nanowires is concentrated from an area of approximately 3,000 μm^2 to 2,000 μm^2. The laser source is filtered out digitally in the images to aid pattern observation.

period of 4 s. It is interesting to note that the silver nanowires are trapped in the laser spot at an angle, as depicted in Fig. 2a. The trapping angle θ_m of silver wires in the OET potential (Fig. 2c) is measured to be approximately $74°$ using the relation $\theta_m = \cos^{-1}(L_t/L_o)$, where L_o equals the total length of the horizontal, non-trapped nanowire and L_t the observed length of the nanowires once they are in the trap. The silver nanowires are trapped in the region of highest electric-field gradient and it is expected that they align to the electric field in that region owing to their high polarizability. Using the simulated values for ∇E^2 (Fig. 2a), we also calculate θ_c, the angle of the electric field in the high-∇E^2 region, and find it to be approximately $64°$, which is within 15% of the experimentally measured value.

As mentioned before, the strength of the DEP force depends on the relative permittivities and conductivities of the nanowire and suspension medium. Therefore, in the case of a comparison of semiconducting (silicon) nanowires and metallic (silver) nanowires, it is expected that the silver nanowires experience a larger DEP force as a result of their higher polarizabilities. Figure 3a shows the maximum trapping speeds achieved for individual silicon and silver nanowires for a range of peak-to-peak a.c. voltages. With an 8-V peak-to-peak a.c. bias applied across the OET device, the silver nanowire experiences speeds up to $125 \mu m \, s^{-1}$ while remaining trapped, whereas the silicon nanowire remains trapped only for speeds $\leq 2 \mu m \, s^{-1}$. Thus, it is possible to separate silicon and silver nanowires by adjusting the scanning speed of the trapping laser while using a suitable peak-to-peak a.c. bias, so that the silver nanowires will be captured by the laser trap and the silicon nanowires will be left behind. Figure 3b–d shows the process of separating an individual silver nanowire from a silicon nanowire. The silver nanowire is aligned with the electric field even at 8 V peak-to-peak as a result of its high polarizability, whereas the silicon nanowire is not aligned. A line laser is used to trap the silicon and silver nanowires (Fig. 3b) and, as the laser is scanned across the stage, the silicon nanowire is left behind (see Supplementary Information, Video S4) but the silver nanowire stays with the trap (Fig. 3d). In addition, control experiments were performed using silicon nanowires of

comparable or larger lengths than the silver nanowires and the same separation effect was observed. We expect this approach to nanowire separation may also be extended to the separation of semiconducting and metallic carbon nanotubes. Despite the smaller cross-sectional area of carbon nanotubes and the r^2 dependence of F_{DEP}, the increased aspect ratio and higher electrical conductivity of carbon nanotubes suggest OET as a promising approach for nanotube separation.

Recently there has been interest in vertically aligned nanowire arrays for solar energy conversion[27], thermoelectric cooling[28] and vertical field-effect transistor[29] applications. One powerful aspect of OET is its ability to perform large-scale assembly of objects with a digital micromirror device (DMD)[3]. Figure 4a,b shows examples of large-scale assembly of nanowires using real-time dynamic trapping. Figure 4a shows the formation of a 5×5 array of single silver nanowires that are individually addressable in real time (see Supplementary Information, Fig. S2, Video S5). Another approach to the formation of large-scale arrays of nanowires is to use larger trapping patterns. Figure 4b shows the process of tuning the density of trapped silver nanowires by varying the size of a rectangular trapping pattern in real time (see Supplementary Information, Video S6). It is interesting to note that when multiple wires are trapped in a single potential, they are observed to repel each other and fill the active trapping pattern owing to dipole–dipole interactions.

At present, many challenges remain before this approach becomes viable for large-scale nanowire integration. Manipulation is restricted to the 2D surface coated by a photoconductive thin film, limiting the construction of three-dimensional (3D) heterostructures. Additionally, wires are observed to adhere to a sample surface through non-specific binding, which limits the ease of manipulation. However, it has been demonstrated recently that nanowire surface functionalization is an effective tool to control interactions between nanowires and surfaces[30] and this method can potentially be used to reduce nanowire adhesion. One promising future direction involves trapping nanowires in lateral directions and immobilization of the nanowires for construction of 3D

heterostructures from metallic and semiconducting nanowires[31]. However, in its present form, real-time OET offers parallel, high-speed manipulation for a broad range of 1D materials, enabling dynamic positioning and rapid separation of semiconducting and metallic nanowires. In principle, the technique may be extended to microfluidic chambers and applied to the separation of other materials, such as carbon nanotubes[17,32], or to the construction of thermoelectric arrays[28].

METHODS

OPTOELECTRONIC TWEEZERS

The OET device consists of a top indium-tin oxide (ITO) transparent electrode and a bottom ITO electrode coated with a 1-μm photoconductive layer of hydrogenated amorphous silicon (a-Si:H). Figure 1a shows the structure of the OET device. The liquid layer containing the nanowire sample is sandwiched between the top and the bottom layers. An a.c. voltage bias is applied between the top and the bottom electrode. To actuate the a-Si:H layer, a 633-nm HeNe laser is used. With no laser present, the voltage drops across the a-Si:H layer. However, once the laser is turned on, it generates electron–hole pairs in the a-Si:H layer and the voltage is transferred to the liquid layer where the laser is present. The voltage in the liquid layer above the illuminated area creates a non-uniform electric-field pattern across the liquid layer.

DYNAMIC TRAP GENERATION

By programming a digital micromirror spatial light modulator (Texas Instruments, 1,024 × 768 pixels, 13.68 μm × 13.68 μm pixel size), it is possible to create real-time, dynamic, flexible trapping patterns for trapping and separating individual nanowires. A 635-nm semiconductor laser was expanded, covering the spatial light modulator area. The spatial light modulator images were controlled through a graphical user interface, which is capable of creating arbitrarily configured real-time traps by focusing the images onto the OET chip surface using a ×10 objective (see Supplementary Information, Videos S5, S6 and S7).

FINITE-ELEMENT ANALYSIS

Simulations of the electric-field gradient produced at virtual electrodes in the OETs were performed with commercial software (COMSOL Multiphysics).

PARTICLE TRACKING ANALYSIS

Nanowire tracking analysis was carried out using the interactive data language (IDL)-based particle-tracking software developed by Crocker and Weeks[33].

SYNTHESIS

The silicon nanowires in Fig. 3 (see also Supplementary Information, Figs S2 and S3) were grown by chemical vapour deposition of $SiCl_4$ onto a silicon wafer, which was gold-coated by electron-beam evaporation of gold in a 850 °C furnace for approximately 30 min (ref. 34). The silicon nanowires used in Fig. 1 (see also Supplementary Information, Figs S4 and S5) were etched from single-crystal silicon wafers following electroless metal deposition[35]. Silver nanowires were prepared using poly(vinyl pyrrolidone) as the capping agent[36] and were found to have diameters of 80–100 nm and lengths of 1–10 μm.

References

1. Xia, Y. N. et al. One-dimensional nanostructures: synthesis, characterization, and applications. Adv. Mater. **15**, 353–389 (2003).
2. Pauzauskie, P. J. & Yang, P. Nanowire photonics. Mater. Today **9**, 36–45 (2006).
3. Chiou, P. Y., Ohta, A. T. & Wu, M. C. Massively parallel manipulation of single cells and microparticles using optical images. Nature **436**, 370–372 (2005).
4. Sirbuly, D. J., Law, M., Yan, H. Q. & Yang, P. D. Semiconductor nanowires for subwavelength photonics integration. J. Phys. Chem. B **109**, 15190–15213 (2005).
5. Law, M. et al. Nanoribbon waveguides for subwavelength photonics integration. Science **305**, 1269–1273 (2004).
6. Kuykendall, T. et al. Crystallographic alignment of high-density gallium nitride nanowire arrays. Nature Mater. **3**, 524–528 (2004).
7. He, R. & Yang, P. Giant piezoresistance effect in silicon nanowires. Nature Nanotech. **1**, 42–46 (2006).
8. Martensson, T. et al. Epitaxial III–V nanowires on silicon. Nano Lett. **4**, 1987–1990 (2004).
9. Ahn, J. H. et al. Heterogeneous three-dimensional electronics by use of printed semiconductor nanomaterials. Science **314**, 1754–1757 (2006).
10. Huang, Y., Duan, X. F., Wei, Q. Q. & Lieber, C. M. Directed assembly of one-dimensional nanostructures into functional networks. Science **291**, 630–633 (2001).
11. Messer, B., Song, J. H. & Yang, P. D. Microchannel networks for nanowire patterning. J. Am. Chem. Soc. **122**, 10232–10233 (2000).
12. Yang, P. Nanotechnology: Wires on water. Nature **425**, 243–244 (2003).
13. Tao, A. et al. Langmuir–Blodgett silver nanowire monolayers for molecular sensing using surface-enhanced Raman spectroscopy. Nano Lett. **3**, 1229–1233 (2003).
14. Jin, S. et al. Scalable interconnection and integration of nanowire devices without registration. Nano Lett. **4**, 915–919 (2004).
15. Sirbuly, D. J. et al. Optical routing and sensing with nanowire assemblies. Proc. Natl Acad. Sci. USA **102**, 7800–7805 (2005).
16. Pauzauskie, P. J. et al. Optical trapping and integration of semiconductor nanowire assemblies in water. Nature Mater. **5**, 97–101 (2006).
17. Krupke, R., Hennrich, F., von Lohneysen, H. & Kappes, M. M. Separation of metallic from semiconducting single-walled carbon nanotubes. Science **301**, 344–347 (2003).
18. Smith, P. A. et al. Electric-field assisted assembly and alignment of metallic nanowires. Appl. Phys. Lett. **77**, 1399–1401 (2000).
19. Lee, S. Y. et al. An electrical characterization of a hetero-junction nanowire (NW) pn diode (n-GaN NW/p-Si) formed by dielectrophoresis alignment. Physica E **36**, 194–198 (2007).
20. Jones, T. B. Electromechanics of Particles (Cambridge Univ. Press, Cambridge, 1995).
21. Ohta, A. T. et al. Dynamic cell and microparticle control via optoelectronic tweezers. J. Micromech. S. **16**, 491–499 (2007).
22. Neale, S. L., Mazilu, M., Wilson, J. I. B., Dholakia, K. & Krauss, T. F. The resolution of optical traps created by light induced dielectrophoresis (LIDEP). Opt. Express **15**, 12619–12626 (2007).
23. Decker, C. Kinetic study and new applications of UV radiation curing. Macromol. Rapid Commun. **23**, 1067–1093 (2002).
24. Beebe, D. J. et al. Functional hydrogel structures for autonomous flow control inside microfluidic channels. Nature **404**, 588–590 (2000).
25. Albrecht, D. R., Tsang, V. L., Saha, R. L. & Bhatia, S. N. Photo- and electropatterning of hydrogel-encapsulated living cell arrays. Lab Chip **5**, 111–118 (2005).
26. Liu, V. A. & Bhatia, S. N. Three-dimensional photopatterning of hydrogels containing living cells. Biomed. Microdev. **4**, 257–266 (2002).
27. Law, M., Greene, L. E., Johnson, J. C., Saykally, R. & Yang, P. Nanowire dye-sensitized solar cells. Nature Mater. **4**, 455–459 (2005).
28. Dresselhaus, M. S. et al. New directions for low-dimensional thermoelectric materials. Adv. Mater. **19**, 1043–1053 (2007).
29. Goldberger, J., Hochbaum, A. I., Fan, R. & Yang, P. Silicon vertically integrated nanowire field effect transistors. Nano Lett. **6**, 973–977 (2006).
30. Yerushalmi, R., Ho, J. C., Jacobson, Z. A. & Javey, A. Generic nanomaterial positioning by carrier and stationary phase design. Nano Lett. **7**, 2764–2768 (2007).
31. Ohta, A. T. et al. Optically controlled cell discrimination and trapping using optoelectronic tweezers. IEEE J. Sel. Top. Quant. Electron. **13**, 235–243 (2007).
32. Arnold, M. S., Green, A. A., Hulvat, J. F., Stupp, S. I. & Hersam, M. C. Sorting carbon nanotubes by electronic structure using density differentiation. Nature Nanotech. **1**, 60–65 (2006).
33. Crocker, J. C. & Weeks, E. R. Particle tracking using IDL ⟨http://www.physics.emory.edu/~weeks/idl/⟩.
34. Hochbaum, A. I., Fan, R., He, R. & Yang, P. Controlled growth of Si nanowire arrays for device integration. Nano Lett. **5**, 457–460 (2005).
35. Peng, K. Q., Yan, Y. J., Gao, S. P. & Zhu, J. Synthesis of large-area silicon nanowire arrays via self-assembling nanoelectrochemistry. Adv. Mater. **14**, 1164–1167 (2002).
36. Sun, Y. G., Gates, B., Mayers, B. & Xia, Y. N. Crystalline silver nanowires by soft solution processing. Nano Lett. **2**, 165–168 (2002).